Desalination and Water Treatment
www.deswater.com
doi: 10.5004/dwt.2021.27688

240 (2021) 191–202
November

Adsorption process of the malachite green onto clay: kinetic and thermodynamic studies

Mohammed Messaoudi[a], Mohamed Douma[a], Najib Tijani[a], Younes Dehmani[b], Lahcen Messaoudi[a,*]

[a]*Laboratory of Materials, Membranes and Nanotechnology, Department of Chemistry, Faculty of Sciences, Moulay Ismail University, PB 11201, Zitoune, Meknes, Morocco, emails: messaoudilahcen56@gmail.com (L. Messaoudi), tmingenierie1@gmail.com (M. Messaoudi), m.douma@yahoo.fr (M. Douma), najibtij@gmail.com (N. Tijani)*
[b]*Laboratory of Chemistry and Biology Applied to the Environment, Faculty of Sciences, Moulay Ismaïl University, PB 11201, Zitoune, Meknes, Morocco, email: dehmaniy@gmail.com*

Received 6 April 2021; Accepted 3 August 2021

ABSTRACT

This work reports the study of the adsorption of malachite green (MG) dye on Moroccan clay according to different parameters impacting the adsorption phenomenon, such as pH, the temperature of the medium and the MG dye concentration. The clay used as adsorbent was initially characterized by X-ray fluorescence spectrometry, Fourier-transform infrared spectroscopy (FTIR), X-ray diffraction, Brunauer–Emmett–Teller, and thermogravimetric analysis. The results indicate that the equilibrium of MG adsorption is reached in 90 min. The efficiency of dye removal on clay increases with the contact time, initial dye concentration, solution temperature and pH. The experimental data obtained were examined using isothermal and kinetic models based on the errors calculated values of R^2 (correlation coefficient) and χ^2 (chi-square). It was found that the nonlinear forms of the Langmuir isotherm and the pseudo-second-order kinetic model are the best-fitting with experimental data. The thermodynamic study showed that the adsorption was a spontaneous and exothermic process. However, FTIR analysis of the adsorbent, before and after MG adsorption, shows that the mechanism of MG adsorption occurs through the phenomenon of chemical interaction between the adsorbate and the adsorbent.

Keywords: Adsorption; Malachite green; Clay; Kinetics; Isotherms; Thermodynamics

1. Introduction

Water is considered an essential element of all socio-economic processes in each country. Because of human ignorance, millions of tons of contamination and poisons have been thrown into the water, and if this is not stopped, there will be increasing pressure on water supplies and therefore on the aquatic environment. These include synthetic organic dyes that are known to be toxic and pathogenic substances suspended in water [1]. They are currently one of the main sources of pollution in water and are widely used in several industries, which causes the introduction of various harmful contaminants into the environment [2,3]. The world production of these dyes is estimated at 1,000 T y^{-1}. The release of this dye into the hydrosphere can damage water quality in several ways, such as dissolved oxygen depletion and other serious consequences [4,5] and all this requires effective and immediate monitoring [6]. Among these dyes, we

* Corresponding author.

Presented at the Second International Symposium on Nanomaterials and Membrane Science for Water, Energy and Environment (SNMS-2021), June 1–2, 2022, Tangier, Morocco

find malachite green (MG), a cationic dye with a triphenylmethane chemical structure. It is used in various fields such as health, food and textiles as a dye or elementary additive and also used as a biocide in aquaculture [6,7]. MG has been shown to cause harmful toxicity not only because of its carcinogenic, genotoxic, mutagenic and teratogenic nature due to the presence of nitrogen in its structure but also because of the visibility of its color in the water, even at low concentrations [6,8,9]. Therefore, the removal of the MG is an essential requirement. Several techniques have been reported in the literature to remove this type of dye from wastewater such as degradation processes, including photocatalytic, photo-oxidative and solar [10], ozonation [11], biological decolorization [12], ultrasonic (US) and electrochemical (EC) [13]. These different treatment processes have advantages but also weaknesses in terms of rates, efficiencies and costs. The adsorption technique has attracted particular attention for the removal of organic pollutants from wastewater because of its simplicity, rapidity of treatment, environmental friendliness and the use of low-cost adsorbents.

Adsorption is a separation process that involves the transfer of mass from the liquid phase (adsorbate) to the inner surface of the solid (adsorbent). The efficiency of this process depends on several parameters such as, the affinity of the adsorbent surface towards the pollutant, which depends in particular on: pH, the temperature of the solution to be treated, the specific surface area of the adsorbent used and the concentration of adsorbate to be analyzed in the solution. Several adsorbents have been used to remove the malachite green dye, including activated carbon [14–16], natural zeolite, silica gel, and seaweed [17], rice husk [18], chitosan–DES beads [19], PMMA/GO and PMMA/GO-Fe_3O_4 nanocomposite [20], aged and virgin nylon microplastics [21], biochar (BC) and activated biochar (ABC) [22], nano-adsorbent derived from eggshell [23]. Relevant research has been undertaken on environmentally friendly, low-cost adsorbents from natural sources with high adsorption potential, large specific surface area, negative charge, cation exchange potential with nanometric size such as clay that lends itself as the good and required adsorbent for dye removal [7,9,24,17].

The objective of the present work is the valorization of a Moroccan clay in the adsorption of the malachite green from aqueous solutions by discontinuous adsorption batch. The clay was characterized by X-ray fluorescence, Fourier-transform infrared spectroscopy (FTIR), X-ray diffraction, thermogravimetric analysis-differential thermal analysis (TGA-DTA), and Brunauer–Emmett–Teller (BET) before any manipulation. In order to optimize the adsorption process, equilibrium isotherms, kinetic data, and thermodynamic studies were calculated and compared. The study of mechanisms was also evaluated on the analysis of the adsorbent before and after adsorption of the MG by FTIR analysis.

2. Materials and methods

2.1. Raw materials

The clay studied is a material that is omnipresent in nature, which makes it competitive with other adsorbents. It is red in color and comes from western Morocco (Taza). This type of clay has never been the subject of a structural and mineralogical study to know its nature. This work will allow the determination of its physicochemical properties and the evaluation of its performance in the adsorption of organic pollutants. The clay was washed and purified by decanting in distilled water and centrifuging for 1 h at 3000 rpm. The resulting clay is then dried at 105°C for 24 h in an oven, then crushed and sieved to a desired grain size fraction using standard ASTM sieves, and the grain size of 63 μm was used in our experiments.

2.2. Dye used

The cationic malachite green dye ($C_{52}H_{54}N_4O_{12}$ (Fig. 1); Mwt 927.02 g mol^{-1}; pKa = 6.9) with purity >90% (Spectrophotometric assay) was purchased from Sigma-Aldrich and has a maximum absorption at a wavelength of 618 nm [9]. Solutions of this dye were prepared by dissolving it in distilled water to the desired concentrations.

2.3. Characterization techniques

Our adsorbent has been characterized by several methods. X-ray fluorescence spectrometry (XRF) was used to determine and measure the concentration of the chemical species in the sample (PANalytical Epsilon 3X spectrometer). The clay sample collected was also subjected to a total mineralogical analysis (disoriented powder) and to an analysis of the mineralogy of the clay fraction (<2 μm) on oriented slides, according to the method of Moore and Reynolds (1989) (X'PERT MPD-PRO powder diffractometer). The BET-specific surface [25] was measured from the adsorption and desorption isotherms of N_2 (ASAP 2010 Micromeritics spectrometer). DTA and TGA thermal analyzes were performed using alumina capsules (TA60 SHIMADZU spectrometer). FTIR spectroscopy was carried out to identify functional groups of the sample (FTIR JASCO 4100). Ultraviolet/visible spectroscopy is used to measure the concentrations of dye (UVmini-1240, Shimadzu brand).

2.4. Cation exchange capacity

The cation exchange capacity of clay allows us to quantify the exchange properties of cations. It gives an idea of the amount of cations that can be replaced by others to compensate for the negative charge of a mass of clay equal to 100 g.

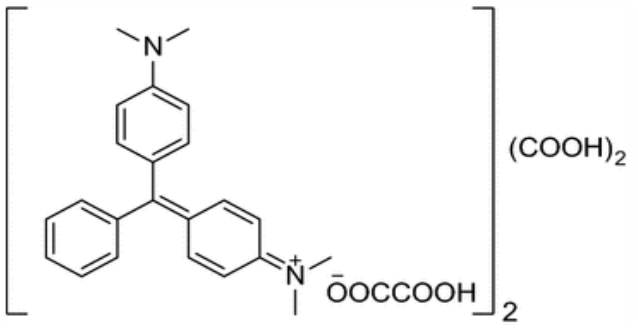

Fig. 1. Structure of malachite green dye.

The cation exchange capacity of clay [26] is determined using a solution of cobalt hexamine chloride, $[Co(NH_3)_6]Cl_3$ with a molar mass of 267.5 g mol^{-1} and purity >98%.

2.5. pH at the point of zero charge

In the interaction between the adsorbate and the adsorbent, the surface charge is an important parameter to the determination of the pH of the charge point remains essential for the understanding of the adsorption phenomenon. The zero point of charge is the pH at which the surface charge due to the H_3O^+ and OH^- ions is canceled. It is noted pHpcn and determined by potentiometric titration. pHpcn represents the limit where the surface charge is zero and changes sign. If the pH is below pHpcn, the net surface charge is positive while for a pH above pHpcn, it is negative [27].

2.6. Adsorption experiments

A series of 250 mL beakers containing 50 mL of a solution of MG was used. After each experiment, the solid–liquid separation was done using a centrifuge at 2600 rpm for 6 min and a syringe filter (0.45 μm). The absorbance of the supernatant solution was measured using a spectrometer (GBC (Ajax, Ontario) (UV/visible 911) at a wavelength corresponding to the maximum absorbance of the MG dye (λ = 620 nm). The effect of the concentration of MG, the pH and the temperature of the solution was studied. The effect of the pH solution was studied by varying the pH in the range of 2–12 with an initial concentration equal to 5 × 10^{-3} mol L^{-1} of the dye. The pH solution was measured using a pH meter (model SL120) and adjusted using a dilute solution of NaOH and HCl. A kinetic study was carried out with a variable contact time between 0–370 min by varying the initial concentration of 10^{-3}–5 × 10^{-4} mol L^{-1}. The adsorption isotherm study was aided in understanding the surface properties of the adsorbent in addition to its interaction towards the adsorbate. Modeling of the adsorption kinetics was undertaken by the pseudo-first-order, pseudo-second-order; whereas, those of isotherms by Langmuir and Freundlich models. To confirm the validity of the proposed kinetic and isothermal models, the error analysis calculations were executed, such as the coefficient of determination (R^2) and chi-square analysis (χ^2) [28,29]. The thermodynamic study consisted in calculating the standard enthalpy, the standard free energy of Gibbs and the standard entropy by varying the temperature solution over a working range according to 303–323 K. The concentration of residual dye in the reaction mixture was calculated using the calibration curve. The equilibrium adsorbed Q_e amount (mg) per unit mass of adsorbent (g) is given by Eq. (1) and all corresponding equations of error functions were summarized as follows:

$$Q_e = \frac{\left(C_i - C_e\right)V}{M} \tag{1}$$

$$\chi^2 = \sum_{i=1}^{n} \frac{\left(q_{\text{ext}} - q_t\right)^2}{q_t} \tag{2}$$

$$R^2 = \frac{\sum_{i=1}^{n}\left(q_t - \overline{q}_{\text{exp}}\right)^2}{\sum_{i=1}^{n}\left(q_t - \overline{q}_{\text{exp}}\right)^2 + \sum_{i=1}^{n}\left(q_t - q_{\text{exp}}\right)^2} \tag{3}$$

where C_i and C_e (mg L^{-1}) were the initial and the residual concentrations of MG, respectively, M (g) is the mass of adsorbent used and V (L) is the volume of MG solution.

3. Results and discussions

3.1. Physico-chemical analyzes of clay (adsorbent)

3.1.1. Chemical composition

The chemical composition in percent by weight of oxides is shown in Table 1. The results obtained indicate that the most abundant oxides in our clay are: SiO_2, Al_2O_3, MgO, Fe_2O_3, CaO and K_2O, Silica (SiO_2) and alumina (Al_2O_3) indicate the high proportion of aluminosilicates. Magnesium (MgO) indicates the presence of dolomite. Potassium (K_2O) confirms the presence of illite, while calcium (CaO) indicates the presence of carbonates (calcite and dolomite). According to Table 1, it can also be seen that the purity of this clay is about 90% and that the impurities represent a percentage of about 8%.

3.1.2. Oriented slides

In an attempt to know the clay minerals existing in our sample, the diffractograms of the four tests are presented in simplified form in Fig. 2. It was observed that illite was characterized by the following peaks located at the position 2θ° = 8.87,17.76 and 26.81. Chlorite is confirmed by peaks located at the position 2θ° = 6.17, 12.4, 18.7 and 25.1 in the following four models: air-dried, solvated with ethylene glycol and heated to 300°C and 550°C. The two peaks located at 2θ° = 12.4 and 25.1, decrease in intensity during the heat treatment at 550°C, confirming the decomposition of kaolinite. Illite and chlorites are therefore not affected by the different treatments [30,31].

Table 1
Chemical composition of clay using XRF analysis

Oxides	Mass (wt.%)
SiO_2	40.67
Al_2O_3	20.83
MgO	11.11
FeO_3	7.02
CaO	4.03
K_2O	4.03
SO_3	1.07
TiO_2	1
P_2O_5	0.43
MnO	0.05
LOI	2.5

Loss on ignition

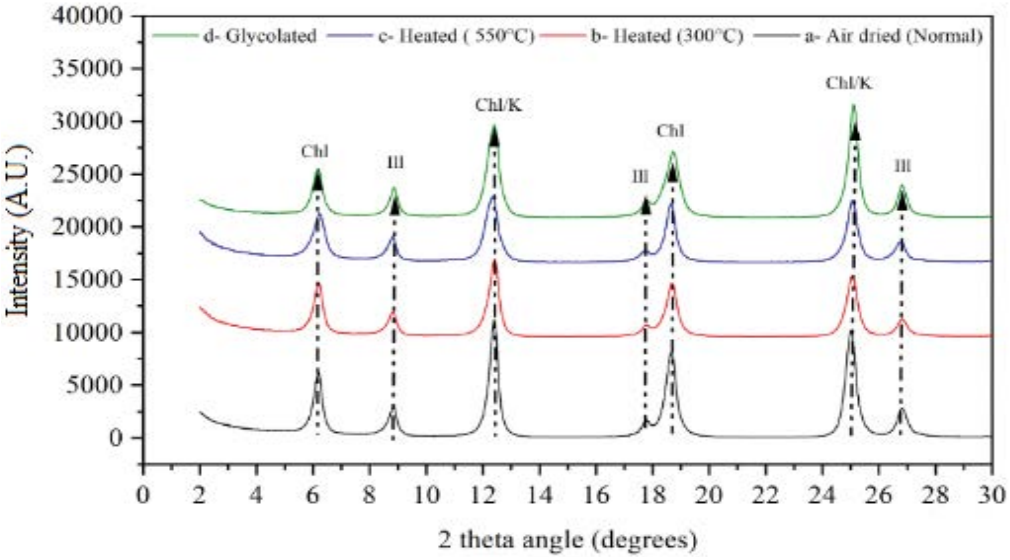

Fig. 2. X-ray diffractograms of oriented slides of clay. Chl: chlorite; Ill: illite; K: kaolinite.

3.1.3. X-ray diffraction analysis

Fig. 3 shows the diffractogram of the studied clay. This one is composed of chlorite, kaolinite, illite, quartz, calcite, and dolomite [30,32,33].

3.1.4. Textural characterization

The adsorption–desorption isotherm obtained for the raw clay is shown in Fig. 4. It is clear that the reversible adsorption–desorption isotherm obtained is similar to type IV according to the IUPAC classification. This type of isotherm characterizes mesoporous. A clear hysteresis loop of type H_3 appears, referring to plate-shaped particles giving rise to slit-shaped pores. The same figure shows the curve of the pore diameter distribution obtained for the clay sample. The latter shows that this diameter varies between 30 and 40 Å with a maximum distribution observed around 38 Å. This indicates the presence of mesoporous in the sample.

3.1.5. Thermogravimetric analysis and differential thermal analysis

The TGA-DTA thermograms of clay are shown in Fig. 5. This analysis revealed a significant weight loss of (–1.656 mg) between 100°C and 1,000°C. DTA shows the existence of an endothermic peak at 141.24°C, this peak has been attributed to the removal of physisorbed water and the interlayer water from the clay mineral with non-swelling clay (illite) [34,35]. The high intensity of the first peak was confirmed by the presence of a non-swelling clay (illite). The second peak appears at 607.55°C corresponding to the dihydroxylation of kaolinite [36,37]. The decomposition of dolomite and calcite is illustrated by a too peaks at around 721.46°C and 845.51°C.

3.1.6. Fourier-transform infrared spectrophotometry

As shown in Fig. 6, the band at 3,562 cm^{-1} is assigned to the stretching vibration of the OH group in clay phase

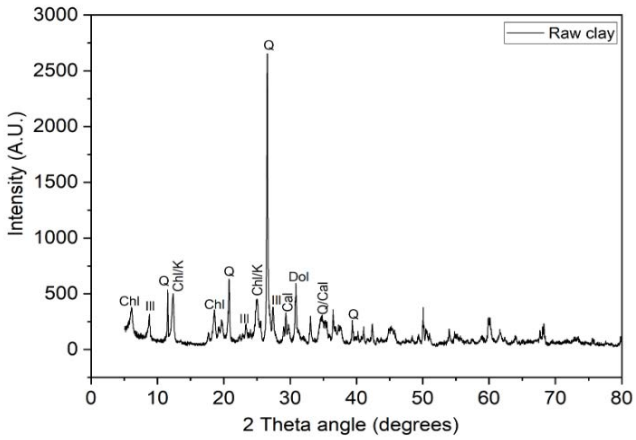

Fig. 3. X-ray diffractogram of raw clay. Chl: chlorite; K: kaolinite; Ill: illite; Q: quartz; Dol: dolomite; Cal: calcite.

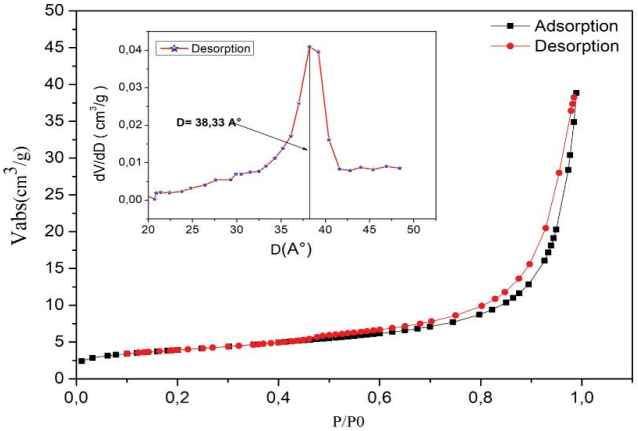

Fig. 4. N_2 adsorption–desorption isotherms of raw clay.

(OH of structural hydroxyls) [38,39]. The bands observed at 3,418; 1,633 cm^{-1} and 1,383 cm^{-1} are due to the stretching and bending vibration of the H_2O adsorbed on the surface and between the clay sheets [37,39,40]. The FTIR spectra reveals a symmetric and asymmetric stretching vibration of the methylene and methyl CH_2, CH_3 group of the aliphatic chain at 2,923 and 2,852 cm^{-1}. The bands observed at 1,435, 878 and 719 cm^{-1} are attributed to the deformation and elongation vibration of the calcite ($CaCO_3$) and quartz [40,41]. The simultaneous presence of the bands around 1,000, 761, and 671 cm^{-1} are attributed respectively to the Si-O elongation vibrations of Si–O–Si and Si–O–Al and this due to the structure of the silicate [34,36]. The bands at 529 and 460 cm^{-1} can be attributed to the stretching vibration of SiO_4^{2-} tetrahedra [37].

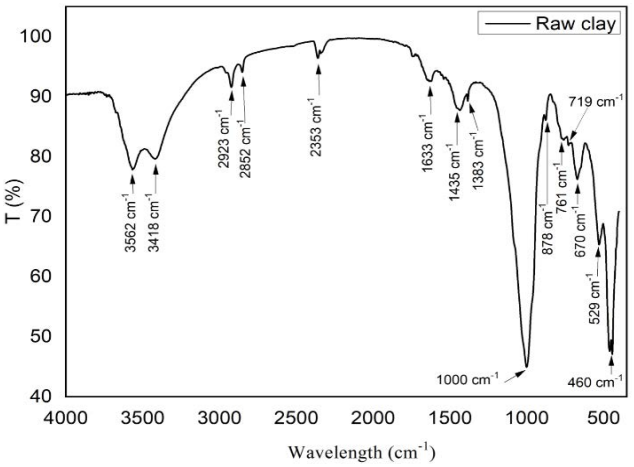

Fig. 6. FTIR spectra of raw clay.

3.2. pH at the point of zero charge and CEC

In this work, the measurements indicate that this material has a zero charge at pH 9 as shown in Fig. 7 and a positive adsorbent surface at pH values below pHpcn and a negative in the opposite state. The CEC of the sample determined by UV-Vis spectroscopy is 75 meq/100 g.

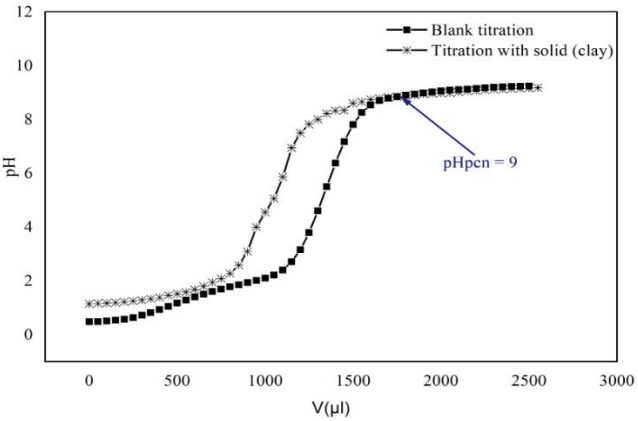

Fig. 7. Zeta potential-pH profile of clay.

3.3. pH effect

The pH solution influences the entire adsorption process and in particular the adsorption capacity, as this parameter affects the structural stability of the clay. Fig. 8 shows the adsorption capacity of the MG by the clay at different pH values. The variation in the adsorption of MG concerning the pH of the medium can be explained based on the surface loading of the adsorbent (clay). In acidic media, the adsorption capacity of MG is low, this could be explained by the fact that the adsorbents are positive carrying the same charge of the cationic dye MG. This can be explained by the accumulation of OH^- ions on the surface of the adsorbent, which favors the adsorption of MG, which carries a

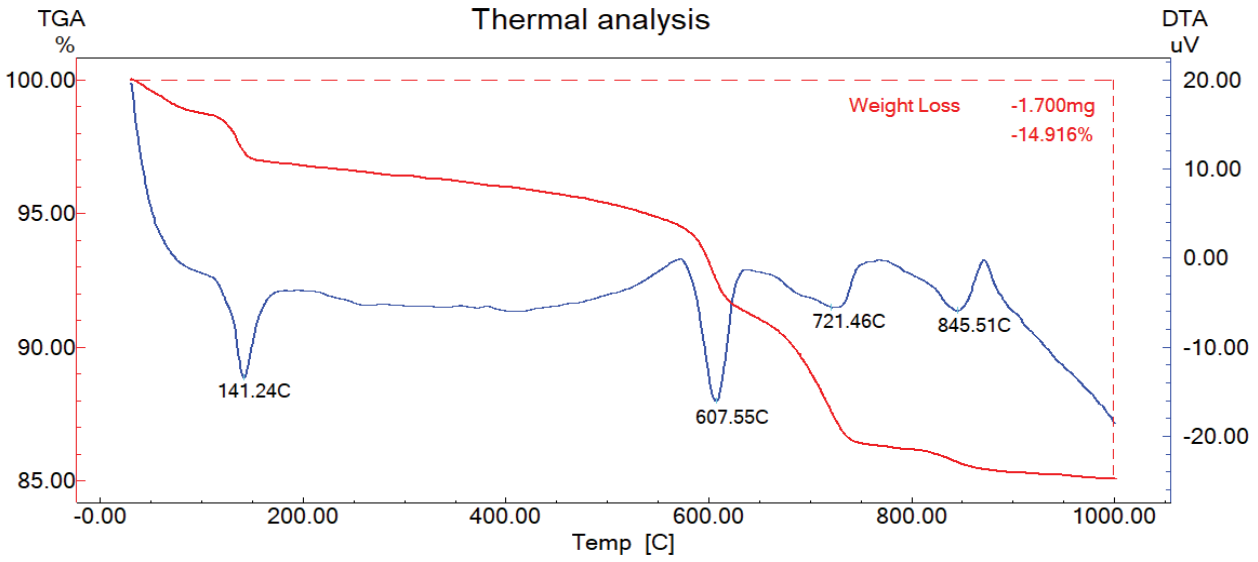

Fig. 5. TGA-DTA thermograms of raw clay.

positive charge on its surface, and therefore the appearance of the phenomenon of electrostatic attraction. And more than the pH > pHpcn, therefore there is an increase in the negative charge density on the surface of the MG, which causes the elimination of MG [42].

3.4. Effect of initial dye concentration and contact time on the MG adsorption process

The initial concentration of MG is considered an important variable and can be attributed to the efficiency of adsorption and removal of the MG. The effect of this parameter is illustrated by the number of effective collisions between the adsorbed molecules and the adsorbing surfaces [43]. Experiments were conducted for initial concentrations of MG ranging from 10^{-3} to 10^{-4} mol L^{-1} at constant temperature and pH. The results in terms of adsorption relative to the initial concentration of MG were presented in Fig. 9. From this figure, it was found that the adsorption capacity of MG by the clay increases with the initial concentration of MG, the latter accelerating the diffusion of the MG dye from the solution onto the clay due to the increased driving force of the concentration gradients [24]. The effect of contact time in the concentration between 10^{-4} and 10^{-3} mol L^{-1} of MG in solution is shown in the same Fig. 9. The curves indicate that the initial concentration has no effect on the contact time which corresponds to the adsorption equilibrium at the adsorbent/adsorbate interface where the support is saturated with the solute. For the adsorbent, the contact time is 30 min, which corresponds to a reduction rate of 56% for the initial concentration of 10^{-4} mol L^{-1} (adsorption capacity of 17 mg g^{-1}), 67% for 5×10^{-4} mol L^{-1} (adsorption capacity of 90 mg g^{-1}) and 80% for a concentration of 10^{-3} mol L^{-1} (adsorption capacity of 180 mg g^{-1}) [16]. The latter value corresponding to the 10^{-3} mol L^{-1} concentration, is among the highest adsorption capacities of MG compared to other types of low-cost adsorbents (Table 2) [9].

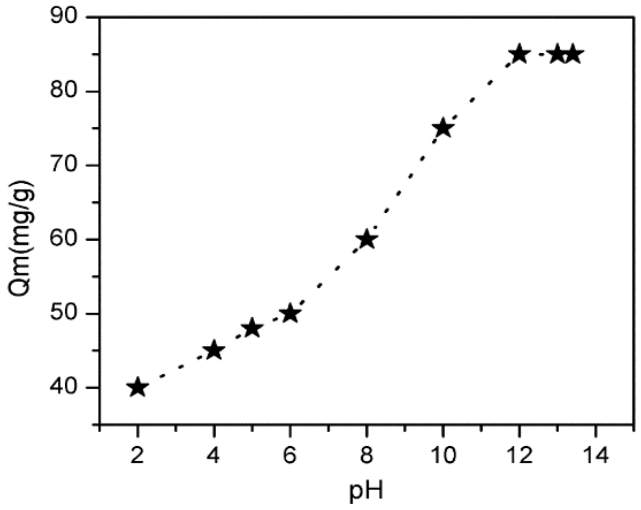

Fig. 8. The adsorption capacity of the MG by the clay at different pH values.

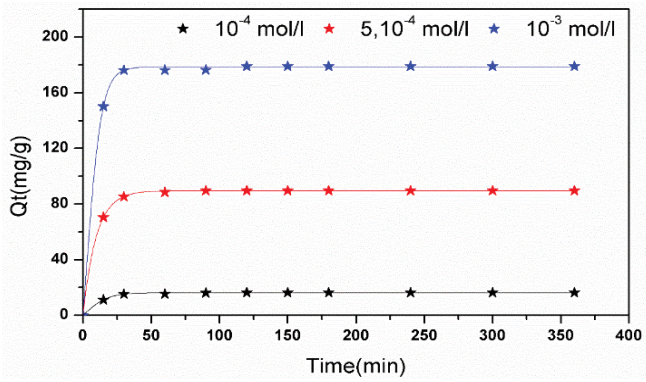

Fig. 9. Effect of contact time on MG adsorption by the clay ($C_0 = 10^{-4}$; 5×10^{-4}; 10^{-3} mol L^{-1}).

3.5. Kinetics of the adsorption process

Adsorption kinetics, expressed in terms of solute retention rate vs. contact time, is one of the most important characteristics defining the evaluation and design of Q_{ads}. In order to correlate the kinetic data, different models were applied to the experimental data obtained from the adsorption process. These are the pseudo-first-order model, the pseudo-second-order model and, the intra-particle model. The linear form of the pseudo-first-order model is illustrated by Eq. (4).

$$\ln\left(Q_e - Q_t\right) = \ln\left(Q_e\right) - k_1 t \tag{4}$$

Eq. (5) of the pseudo-second-order model used to simulate the kinetic adsorption behavior of MG is written as follows:

$$\frac{t}{Q_e} = \frac{1}{Q_e^2 K_2} + \frac{1}{Q_e} t \tag{5}$$

where Q_e and Q_t (mg g^{-1}) are the amounts of MG dye adsorbed at equilibrium and time t (min) respectively, K_1 (min^{-1}) and K_2 (g mg^{-1} min^{-1}) are the pseudo-first and pseudo-second-order adsorption rate constants, respectively [16,42]. Fig. 10 shows the absorption of MG vs. time at different concentrations. According to this figure, the adsorption rate of MG on clay increases rapidly in the first period ($t < 90$ min) due to the availability of clay surface adsorption sites, then, thereafter it becomes continuous. The kinetic parameters obtained from the two models are summarized in Table 3. The results obtained show that the R^2 values for the pseudo-second-order ($R^2 = 0.99$) were higher than those for the pseudo-first-order ($R^2 = 0.89$), moreover, the values of Chi-square χ^2 for the pseudo-second-order model are lower than those of the pseudo-first-order model. Thus, the adsorption kinetics followed the pseudo-second-order model which suggests that adsorption depends on the adsorbate-adsorbent pair. It has been successfully applied in a number of MG systems [53].

The Weber–Morris intraparticle model was tested to identify the mechanism of diffusion of the MG dye from the

Table 2
Comparison of MG adsorption capacity with other low-costs absorbents

Adsorbent	MG adsorption capacity (mg g^{-1})	Ref
Clay	180	This work
Banana (*Musa paradisiaca*) stalk-based activated carbon	141.76	[44]
Rice husk activated carbon (RHAC)	49.62	[45]
Pomelo (*Citrus grandis*) peels	178.43	[46]
Centaurea solstitialis (CS) plants	91	[47]
Conch shell powder (CSP)	92.25	[48]
Luffa acutangula peel	69.64	[49]
Fly ash	40.65	[50]
Low-cost inorganic powder (Persian kaolin)	52.91	[51]
Pleurotus ostreatus (A macro-fungus)	125.00	[52]

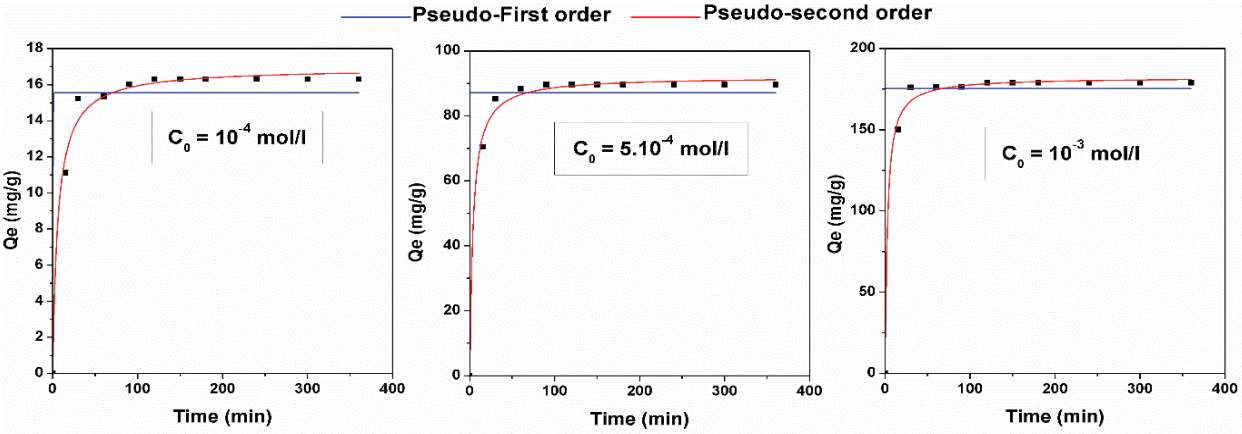

Fig. 10. Adsorption kinetics with nonlinear models of pseudo-first and pseudo-second-order for MG onto clay at different initial dye concentrations (C_0 = 10^{-4}; 5 × 10^{-4}; 10^{-3} mol L^{-1}).

Table 3
Parameters of pseudo-first-order and pseudo-second-order models

		Pseudo-first-order				Pseudo-second-order			
C_0 (mol L^{-1})	$Q_{t,exp}$ (mg g^{-1})	χ^2	K_1 (min^{-1})	R^2	Q_e (mg g^{-1})	χ^2	K_2 (g mg^{-1} min^{-1})	R^2	Q_e (mg g^{-1})
10^{-4}	16.31	2.60	3.71	0.89	15.56	0.27	0.009	0.99	16.92
5 × 10^{-4}	89.64	36.37	16.93	0.94	87.17	3.58	0.0084	0.99	92
10^{-3}	179.07	79.95	33.8	0.96	175.35	12.2	0.002	0.99	182.22

solution to the inner and outer surfaces of the adsorbent. The rate parameter for intraparticle diffusion is expressed as follows:

$$Q_t = k_{id} \times t^{1/2} \quad (6)$$

where k_{id} (mg g^{-1} $min^{-1/2}$)) is the intraparticle diffusion rate constant. The validity of the intraparticle diffusion model was tested at different temperatures. Fig. 11 shows the adsorbed quantity Q_t vs. $t^{1/2}$ for the three concentrations studied. The parameters related to this analysis are summarized in Table 4. Fig. 11 shows that the plots are not linear over the whole time interval of the study which suggests that the adsorption of MG on our clay follows two steps. The first stage is quickly from where the adsorption is done on the external surface of the clay adsorbate followed by a second stage which is late from where the diffusion of the molecules is done in the internal mesoporous of the clay. According to Table 3, the K_{id1} values are higher than K_{id2}, and the value of the correlation coefficient R^2 is equal to 0.99, indicating that when the molecules of the MG dye diffuse through the internal pores or along the surface wall of the pores in the clay particles, the diffusion resistance increases, resulting in a decrease in the diffusion rate.

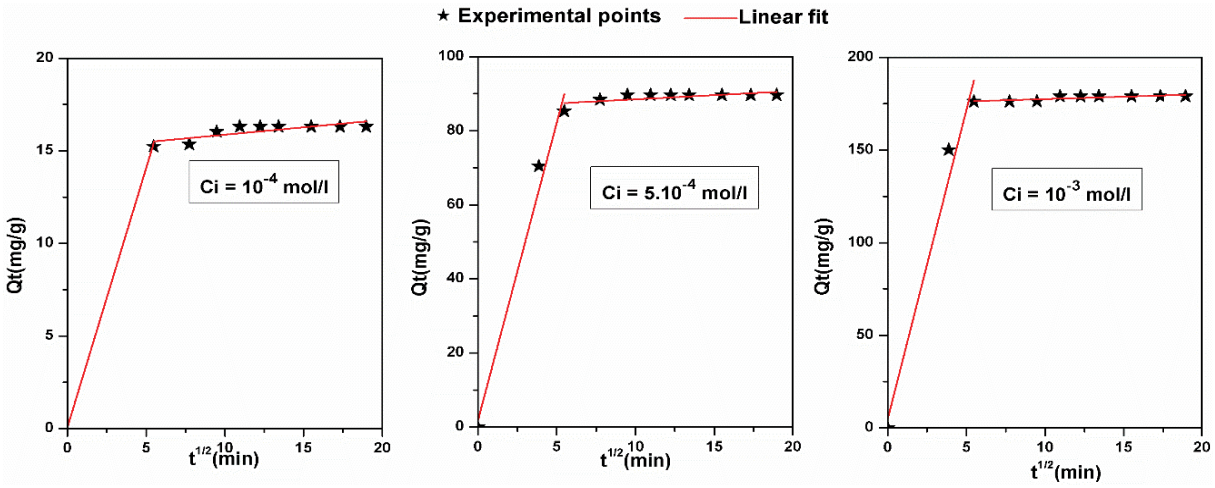

Fig. 11. Intraparticle diffusion model for MG adsorption on clay.

Table 4
Intraparticle diffusion parameters of MG on clay

	Step 1			Step 2		
C_i (mol L^{-1})	R^2	K_{id1} (mg g^{-1} $min^{1/2}$)	C_i (mg g^{-1})	R^2	K_{id2} (mg g^{-1} $min^{-1/2}$)	C_i (mg g^{-1})
10^{-4}	0.99	2.79	0.064	0.59	0.08	15.06
5×10^{-4}	0.96	16.05	1.87	0.68	0.22	86.27
10^{-3}	0.95	33.39	4.72	0.61	0.25	175.01

3.6. Adsorption isotherms

The adsorption isotherm tends to explain any interaction between the adsorbate and the adsorbent, determine the maximum adsorbate binding capacities and also define the type of adsorption [54]. In this work, two well-known models of isotherms were evaluated; Langmuir and Freundlich [54,55]. The form of the Freundlich [Eq. (7)] and Langmuir [Eq. (8)] equations are as follows:

$$Q_e = K_f \times C_e \times \frac{1}{n} \tag{7}$$

$$\frac{C_e}{Q_e} = \frac{1}{Q_m \times K_L} + \frac{C_e}{Q_m} \tag{8}$$

where K_f is the adsorption capacity, n is the adsorption intensity, Q_e is the amount of solute adsorbed per unit mass of adsorbent at equilibrium (mg g^{-1}), C_e (mg L^{-1}) is the residual concentration at equilibrium, Q_m (mg g^{-1}) is the adsorbed amount at equilibrium, and K_L (L mg^{-1}) represents the ratio of the rate constant of adsorption and desorption.

Fig. 12 shows the plots of C_e/Q_e vs. C_e and the plots of $\ln(Q_e)$ vs. $\ln(C_e)$ for the adsorption of MG on clay at temperatures ranging from 30°C to 50°C, according to the linear forms of the Freundlich and Langmuir isotherm. Similarly, as the kinetic studies studied, the values of the constants calculated (R^2, χ^2) from the linear forms of the two isotherms are given in Table 4. It has been observed that the values of the coefficient of determination R^2, were in a range between 0.90 and 0.98 for the Freundlich isotherm, while for the Langmuir isotherm, they were between 0.86 and 0.99, and the values of Chi-square χ^2 for the Langmuir model are lower than of the Freundlich model, which proves that the isotherm was linear over the whole range of temperatures studied with a good linear correlation coefficient close to 1 [56]. This confirms the monolayer coverage of the MG dye on the clay surface and the homogeneous distribution of the active sites on the adsorbent [55], and as shown in Table 5, Q_m and K_f values increase with increasing temperature, indicating that the adsorption process is endothermic in nature.

3.7. Thermodynamic analysis

Adsorption is a phenomenon that can be endothermic or exothermic depending on the adsorbent material and the nature of the adsorbed molecules. To assess the effect of temperature on the adsorption of MG by our clay, the study of real thermodynamic parameters (($\Delta H°$, $\Delta S°$, $\Delta G°$) was carried out at different temperatures (303.15, 313.15, and 323.15 K).

The values of Gibbs' free energy variation ($\Delta G°$), enthalpy variation ($\Delta H°$), and entropy variation ($\Delta S°$) were calculated using the following equation:

$$\ln K_1 = -\frac{\Delta H°}{RT} + \frac{\Delta S°}{R} \tag{9}$$

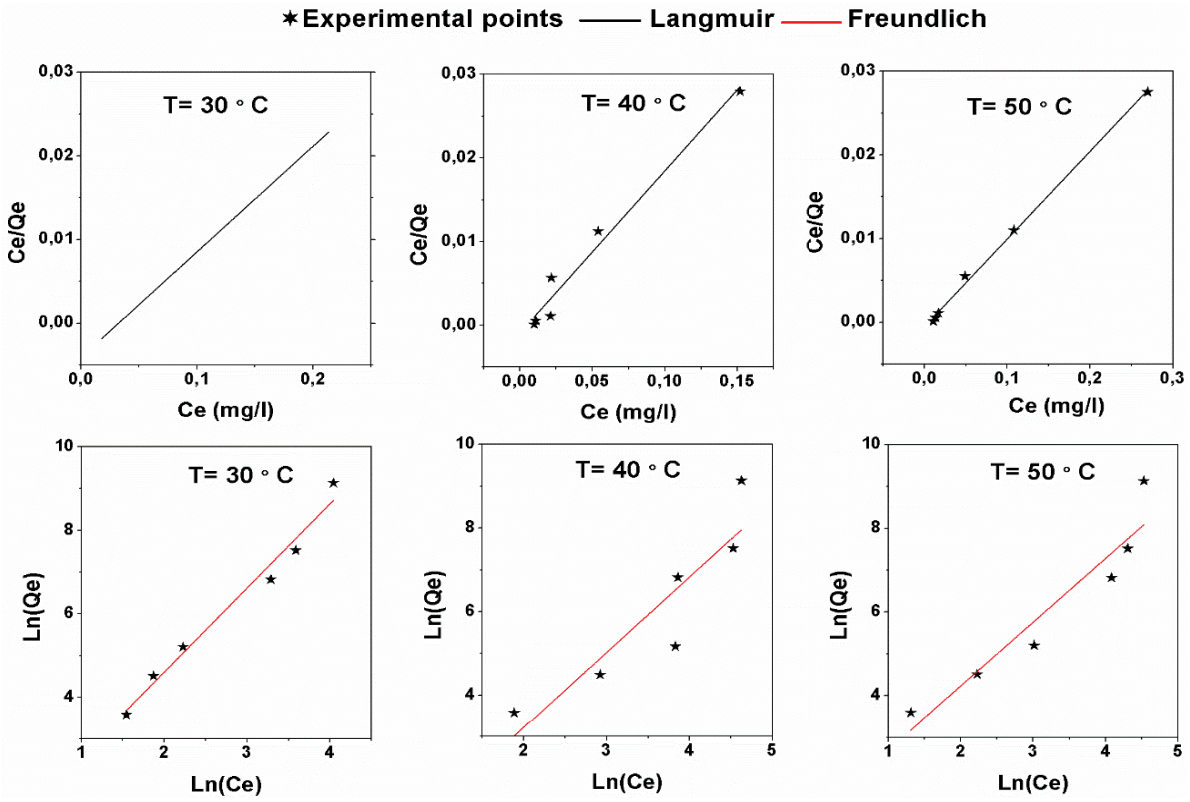

Fig. 12. Adsorption isotherms of MG onto clay at different temperatures (T = 30°C, 40°C and 50°C) with adjustment of the Langmuir and Freundlich linear models.

Table 5
Freundlich and Langmuir parameters obtained for the adsorption of MG on the clay at various temperatures

	T (°C)	30	40	50
Langmuir	Q_m (mg g^{-1})	31.25	65.21	125.36
	K_L (L mg^{-1})	5.15	7.93	10.01
	R^2	0.93	0.96	0.99
	χ^2	0.02	0.01	0.002
Freundlich	K_f (mg g^{-1})	0.30	0.40	0.68
	$1/n$	0.57	1.80	1.97
	R^2	0.90	0.90	0.98
	χ^2	0.15	0.42	0.24

where R is the universal gas constant, T is the absolute solution temperature and K_L is the Langmuir constant.

Fig. 13 represents the plot of $\ln(K_L)$ vs. $1/T$ and the parameters studied are shown in Table 6. The positive value of $\Delta H°$ (27.092 kJ mol) obtained in this work indicates that the adsorption is an endothermic process. The positive value of $\Delta S°$ (103.30 J K^{-1} mol^{-1}) implies that there have been structural exchanges between the active sites of the adsorbent and the MG and this reflects the affinity of the clay towards the MG. On the other hand, the negative values of the free energy $\Delta G°$ show that the adsorption of MG on the clay adsorbent is thermodynamically spontaneous, we can also observe that the values of $\Delta G°$ decrease

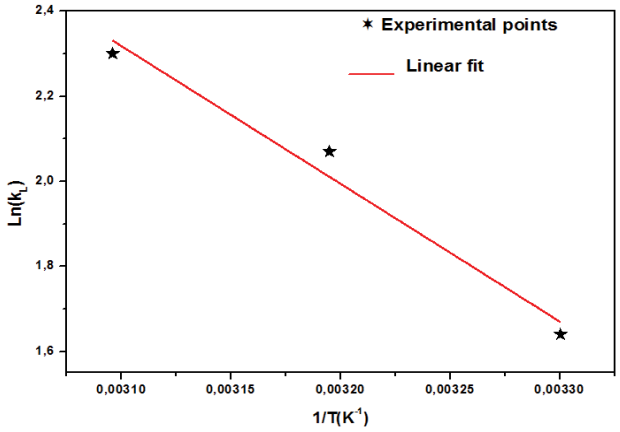

Fig. 13. Graph of $\ln K_L$ (K_L is the Langmuir constant) vs. $1/T$ for the adsorption of MG on clay.

with increasing temperature, this means a better adsorption efficiency at higher temperatures.

3.8. Adsorption mechanism

The characterization of the solid before and after the MG adsorption has been carried out by the FTIR technique. It can help us to determine the mechanism suggested by the fixation of the adsorbed molecules on the solid and to reveal the changes in vibrational bonds, which can occur

Table 6
Thermodynamic parameters of MG adsorption on clay at different temperatures

T (K)	$\Delta S°$ (J K^{-1} mol^{-1})	$\Delta H°$ (kJ mol^{-1})	$\Delta G°$ (kJ mol^{-1})
303.15			–4.201
313.15	103.30	27.092	–5.231
323.15			–6.267

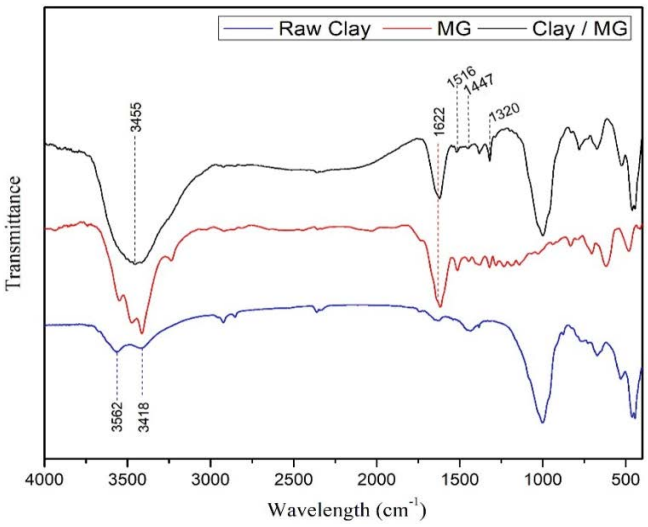

Fig. 14. FTIR spectra of clay before and after MG adsorption.

during each adsorption process. Several mechanisms in the literature find a place in the explanation of the adsorption phenomenon such as (electrostatic interaction, complexation, hydrogenation, and chemical interactions, etc.), in our case, we observed in Fig. 14 the characteristic stretching vibration band of the OH group of the clay phase (OH of the structural hydroxyl) located at 3,562 cm^{-1} changed shape after MG adsorption due to the penetration of MG into the intermediate layer of the kaolinite. Besides, the adsorption band of 1,622 cm^{-1} which is mostly a υCOO (the amide I), suggesting the existence of dipolar interactions between the negative charge of the carboxylate group and MG as a cationic dye, the H-bonding interaction and the dipole–dipole H-bonding interaction. The new bands, linked to the band vibrations of the MG molecules, appear at 1,516 cm^{-1}, 1,447 and 1,320 cm^{-1} are due to the bending vibration of the C-H bond in the methyl groups, the aromatic part and amide II, respectively [57,58]. These bands indicate that the MG reacted with the clay surface and new bonds were formed between the MG and the clay. All these findings indicate that a chemical adsorption has occurred.

4. Conclusions

The present study examined the successful removal of cationic malachite green dye in an aqueous solution using a powerful, inexpensive and environmentally friendly adsorbent. The effect of the initial concentration of the dye and the contact time on its adsorption process was studied. It was found that the adsorption capacity of MG by clay increases with its initial concentration (adsorption capacity of 180 mg g^{-1} for an initial concentration of 10^{-3} mol L^{-1}).

The experimental data provided by the kinetics studies indicated that the pseudo-second-order model is the most appropriate for dye adsorption, while the equilibrium data was well associated with Langmuir isotherm.

The results obtained from the thermodynamic study showed that the adsorption of MG dye was spontaneous ($\Delta G° < 0$) and endothermic ($\Delta H° > 0$) in nature.

References

[1] Kh. Rostami, M.R. Joodaki, Some studies of cadmium adsorption using *Aspergillus niger*, *Penicillium austurianum*, employing an airlift fermenter, Chem. Eng. J., 89 (2002) 239–252.
[2] S.J. Culp, L.R. Blankenship, D.F. Kusewitt, D.R. Doerge, L.T. Mulligan, F.A. Beland, Toxicity and metabolism of malachite green and leucomalachite green during short-term feeding to Fischer 344 rats and B6C3F1 mice, Chem. Biol. Interact., 122 (1999) 153–170.
[3] A.K.T. Mohammad, A.S. Abdulhameed, A.H. Jawad, Box–Behnken design to optimize the synthesis of new crosslinked chitosan-glyoxal/TiO_2 nanocomposite: methyl orange adsorption and mechanism studies, Int. J. Biol. Macromol., 129 (2019) 98–109.
[4] A.H. Jawad, R. Razuan, J.N. Appaturi, L.D. Wilson, Adsorption and mechanism study for methylene blue dye removal with carbonized watermelon (*Citrullus lanatus*) rind prepared via one-step liquid phase H_2SO_4 activation, Surf. Interfaces, 16 (2019) 76–84.
[5] N. Mohammadi, H. Khani, V.K. Gupta, E. Amereh, S. Agarwal, Adsorption process of methyl orange dye onto mesoporous carbon material-kinetic and thermodynamic studies, J. Colloid Interface Sci., 362 (2011) 457–462.
[6] S. Srivastava, R. Sinha, D. Roy, Toxicological effects of malachite green, Aquat. Toxicol., 66 (2004) 319–329.
[7] R. Ahmad, R. Kumar, Adsorption studies of hazardous malachite green onto treated ginger waste, J. Environ. Manage., 91 (2010) 1032–1038.
[8] G.K. Parshetti, S.G. Parshetti, A.A. Telke, D.C. Kalyani, R.A. Doong, S.P. Govindwar, Biodegradation of Crystal Violet by agrobacterium radiobacter, J. Environ. Sci., 23 (2011) 1384–1393.
[9] N.P. Raval, P.U. Shah, N.K. Shah, Malacite green "a cationic dye" and its removal from aqueous solution by adsorption, Appl. Water Sci., 7 (2017) 3407–3445.
[10] L. Saikia, D. Bhuyan, M. Saikia, B. Malakar, D.K. Dutta, P. Sengupta, Photocatalytic performance of ZnO nanomaterials for self-sensitized degradation of malachite green dye under solar light, Appl. Catal., A, 490 (2015) 42 –49.
[11] X.J. Zhou, W.Q. Guo, S.S. Yang, H.S. Zheng, N.Q. Ren, Ultrasonic-assisted ozone oxidation process of triphenylmethane dye degradation: evidence for the promotion effects of ultrasonic on malachite green decolorization and degradation mechanism, Bioresour. Technol., 128 (2013) 827–830.
[12] G.Y. Lv, J.H. Cheng, X.Y. Chen, Z.F. Zhang, L.F. Fan, Biological decolorization of malachite green by *Deinococcus radiodurans* R1, Bioresour. Technol., 144 (2013) 275–280.
[13] Q. Ren, C. Kong, Z. Chen, J. Zhou, W. Li, D. Li, Z. Cui, Y. Xue, Y. Lu, Ultrasonic assisted electrochemical degradation of malachite green in wastewater, Microchem. J., 164 (2021) 106059, doi: 10.1016/j.microc.2021.106059.
[14] A. Özcan, Ç. Ömeroğlu, Y. Erdoğan, A.S. Özcan, Modification of bentonite with a cationic surfactant: an adsorption study of textile dye Reactive Blue 19, J. Hazard. Mater., 140 (2007) 173–179.
[15] A.A. Ahmad, M.A. Ahmad, N.K.E.M. Yahaya, J. Karim, Adsorption of malachite green by activated carbon derived from gasified Hevea brasiliensis root, Arabian J. Chem., 4 (2021)103104, doi: 10.1016/j.arabjc.2021.103104.

[16] W. Qu, T. Yuan, G. Yin, S. Xu, Q. Zhang, H. Su, Effect of properties of activated carbon on malachite green adsorption, Fuel, 249 (2019) 45–53.
[17] B. Samiey, A.R. Toosi, Adsorption of malachite green on silica gel: effects of NaCl, pH and 2-propanol, J. Hazard. Mater., 184 (2010) 739–745.
[18] S. Chowdhury, R. Mishra, P. Saha, P. Kushwaha, Adsorption thermodynamics, kinetics and isosteric heat of adsorption of malachite green onto chemically modified rice husk, Desalination, 265 (2011) 159–168.
[19] A.C. Sadiq, N.Y. Rahim, F.B. Mohd Suah, Adsorption and desorption of malachite green by using chitosan-deep eutectic solvents beads, Int. J. Biol. Macromol., 164 (2020) 3965 –3973.
[20] M. Rajabi, K. Mahanpoor, O. Moradi, Preparation of PMMA/GO and PMMA/GO Fe_3O_4 nanocomposites for malachite green dye adsorption: kinetic and thermodynamic studies, Composites, Part B, 167 (2019) 544–555.
[21] L. Lin, S. Tang, X. Wang, X. Sun, A. Yu, Adsorption of malachite green from aqueous solution by nylon microplastics: reaction mechanism and the optimum conditions by response surface methodology, Process Saf. Environ. Prot., 140 (2020) 339–347.
[22] M. Choudhary, R. Kumar, S. Neogi, Activated biochar derived from *Opuntia ficus*-indica for the efficient adsorption of malachite green dye, Cu^{+2} and Ni^{+2} from water, J. Hazard. Mater., 392 (2020) 122441, doi: 10.1016/j.jhazmat.2020.122441.
[23] A. Moosavi, A.A. Amooey, A. Alinejad Mir, M.H. Marzbali, Extraordinary adsorption of acidic fuchsine and malachite green onto cheap nano-adsorbent derived from eggshell, Chin. J. Chem. Eng., 28 (2020) 1591–1602.
[24] E. Bulut, M. Özacar, I.A. Şengil, Adsorption of malachite green onto bentonite: Equilibrium and kinetic studies and process design, Microporous Mesoporous Mater., 115 (2008) 234–246.
[25] E. Barrett, L.G. Joyner, P.P. Halenda, The volume and area distrbutions in porous substances, J. Am. Chem. Soc., 73 (1951) 373–380.
[26] D. Aran, A. Maul, J. Masfaraud, A spectrophotometric measurement of soil cation exchange capacity based on cobaltihexamine chloride absorbance, C.R. Geosci., 340 (2008) 865–871.
[27] A. Dehbi, Y. Dehmani, H. Omari, A. Lammini, K. Elazhari, A. Abdallaoui, Hematite iron oxide nanoparticles (α-Fe_2O_3): synthesis and modelling adsorption of malachite green, J. Environ. Chem. Eng., 8 (2019) 103394, doi: 10.1016/j.jece.2019.103394.
[28] H.N. Tran, S.J. You, H.P. Chao, Effect of pyrolysis temperatures and times on the adsorption of cadmium onto orange peel derived biochar, Waste Manage. Res., 34 (2016) 129–138.
[29] H.N. Tran, Y.F. Wang, S.J. You, H.P. Chao, Insights into the mechanism of cationic dye adsorption on activated charcoal: the importance of Π–Π interactions, Process Saf. Environ. Prot., 107 (2017) 168–180.
[30] G. Jozanikohan, F. Sahabi, G.H. Norouzi, H. Memarian, B. Moshiri, Quantitative analysis of the clay minerals in the Shurijeh Reservoir Formation using combined X-ray analytical techniques, Russ. Geol. Geophys., 57 (2016) 1048–1063.
[31] S. Khemakhem, Thèse de Doctorat: Préparation de membranes à base d'argile tunisienne, 2005.
[32] H. Ouallal, Y. Dehmani, H. Moussout, L. Messaoudi, Kinetic, isotherm and mechanism investigations of the removal of phenols from water by raw and calcined clays, Heliyon, 5 (2019) e01616.
[33] N. Ouis, N. Benharrats, M. Belbachir, Tamazert kaolin as catalyst in synthesis of polytetrahydrofuran, C.R. Chim., 7 (2004) 955–962.
[34] A. Majouli, S.A. Younssi, S. Tahiri, A. Albizane, H. Loukili, M. Belhaj, Characterization of flat membrane support elaborated from local Moroccan Perlite, Desalination, 277 (2011) 61–66.
[35] Y. Sedjro, T. Kiki, Caractérisation minéralogique, thermique et microscopique des sols fins en technique routière, HAL Id: tel-01476079 Docteur de l' Université de Bordeaux et de l' Université d' Abomey – Calavi, 2017.
[36] F. Chargui, Synthese et caracterisation d'une mullite à base de matieres locales pour substrats de silicium photovoltaïque, U. F. Abbas-setif. Available at: http://dspace.univ-setif.dz:8888/jspui/handle/123456789/2650 (2018)
[37] R.S. Nicolas, M. Cyr, G. Escadeillas, Characteristics and applications of flash metakaolins, Appl. Clay Sci., 83 (2013) 253–262.
[38] A. Bouazizi, S. Saja, B. Achiou, M. Ouammou, J.I. Calvo, A. Aaddane, S.A. Younssi, Elaboration and characterization of a new flat ceramic MF membrane made from natural Moroccan bentonite. Application to treatment of industrial wastewater, Appl. Clay Sci., 132 (2016) 33–40.
[39] D. Hank, Z. Azi, S. Ait Hocine, O. Chaalal, A. Hellal, Optimization of phenol adsorption onto bentonite by factorial design methodology, J. Ind. Eng. Chem., 20 (2014) 2256–2263.
[40] F. Ayari, E. Srasra, M. Trabelsi-Ayadi, Characterization of bentonitic clays and their use as adsorbent, Desalination, 185 (2005) 391–397.
[41] J.R.O. Kikouama, K.L. Konan, A. Katty, J.P. Bonnet, L. Baldé, N. Yagoubi, Physicochemical characterization of edible clays and release of trace elements, Appl. Clay Sci., 43 (2009) 135–141.
[42] R. Bagheri, M. Ghaedi, A. Asfaram, E. Alipanahpour Dil, H. Javadian, RSM-CCD design of malachite green adsorption onto activated carbon with multimodal pore size distribution prepared from *Amygdalus scoparia*: kinetic and isotherm studies, Polyhedron, 171 (2019) 464–472.
[43] B. Enayatpour, M. Rajabi, M. Yari, S.M.R. Mirkhan, F. Najafi, O. Moradi, A. Agarwal, V.K. Gupta, Adsorption/desorption study of proteins onto multi-walled carbon nanotubes and amino multi-walled carbon nanotubes surfaces as adsorbents, J. Mol. Liq., 231 (2017) 566–571.
[44] O.S. Bello, M.A. Ahmad, N. Ahmada, Adsorptive features of banana (*Musa paradisiaca*) stalk-based activated carbon for malachite green dye removal, Chem. Ecol., 28 (2012) 153–167.
[45] Y.C. Sharma, Adsorption Characteristics of a low-cost activated carbon for the reclamation of colored effluents containing malachite green, J. Chem. Eng. Data, 56 (2011) 478–484.
[46] O.S. Bello, M.A. Ahmad, B. Semire, Scavenging malachite green dye from aqueous solutions using pomelo (*Citrus grandis*) peels: kinetic, equilibrium and thermodynamic studies, Desal. Water. Treat., 56 (2014) 521–535.
[47] M. Saleh, M. Yalvaç, H. Arslan, M. Gün, Malachite green dye removal from aqueous solutions using invader *Centaurea solstitialis* plant and optimization by response surface method: kinetic, isotherm, and thermodynamic study, Eur. J. Sci. Technol., 7 (2019) 755–768.
[48] S. Chowdhury, P.D. Saha, Mechanistic, Kinetic, and thermodynamic evaluation of adsorption of hazardous malachite green onto conch shell powder, Sep. Sci. Technol., 46 (2011) 1966–1976.
[49] H.W. Ng, L.Y. Lee, W.L. Chan, S. Gan, N. Chemmangattuvalappil, *Luffa acutangula* peel as an effective natural biosorbent for malachite green removal in aqueous media: equilibrium, kinetic and thermodynamic investigations, Desal. Water Treat., 57 (2016) 7302–7311.
[50] A. Witek-Krowiak, R.G. Szafran, S. Modelski, A. Dawiec, Removal of cationic dyes from aqueous solutions using microspherical particles of fly ash, water, Environ. Res., 84 (2012) 162–169.
[51] A.R. Tehrani-Bagha, H. Nikkar, N.M. Mahmoodi, M. Markazi, F.M. Menger, The sorption of cationic dyes onto kaolin: kinetic, isotherm and thermodynamic studies, Desalination, 266 (2011) 274–280.
[52] Z. Chen, H. Deng, C. Chen, Y. Yang, H. Xu, Biosorption of malachite green from aqueous solutions by *Pleurotus ostreatus* using Taguchi method, J. Environ. Health Sci. Eng., 12 (2014), doi: 10.1186/2052-336X-12-63.
[53] L. Zhao, W. Lv, J. Hou, Y. Li, J. Duan, S. Ai, Synthesis of magnetically recyclable g-C_3N_4/Fe_3O_4/ZIF-8 nanocomposites for excellent adsorption of malachite green, Microchem. J., 152 (2020) 104425, doi: 10.1016/j.microc.2019.104425.
[54] A.A. Hendi, M. Rashad, Photo-induced changes in nano-copper oxide for optoelectronic applications, Z. Phys. B: Condens. Matter, 538 (2018) 185–190.

[55] Y. Sa, Y. Aktay, Application of equilibrium and mass transfer models to dynamic removal of Cr(VI) ions by chitin in packed column reactor, Process Biochem., 36 (2001) 1187–1197.
[56] M.R. Abukhadra, M.A. Sayed, A.M. Rabie, S.A. Ahmed, Surface decoration of diatomite by Ni/NiO nanoparticles as hybrid composite of enhanced adsorption properties for malachite green dye and hexavalent chromium, Colloids Surf., A, 577 (2019) 583–593.
[57] V.M. Muinde, J.M. Onyari, B. Wamalwa, J. Wabomba, R.M. Nthumbi, Adsorption of Malachite Green from aqueous solutions onto rice husks: kinetic and equilibrium studies, J. Environ. Prot., 8 (2017) 215–230.
[58] H. Omar, A. El-gendy, K. Al-Ahmary, Bioremoval of toxic dye by using different marine macroalgae, Turk. J. Bot., 42 (2018) 15–27.